https://doi.org/10.5194/egusphere-2025-4223
Preprint. Discussion started: 4 September 2025

What caused record-breaking aerosol loading over the South China Sea in April 2023

Saginela Ravindra Babu[1*] and Neng-Huei Lin[1,2*]

[1]Department of Atmospheric Sciences, National Central University, Taoyuan 32001, Taiwan.

[2]Center for Environmental Monitoring and Technology, National Central University, Taoyuan 32001, Taiwan.

Correspondence to**:** S. Ravindra Babu (baburavindra595@gmail.com) and Neng-Huei Lin (nhlin@cc.ncu.edu.tw).

Abstract:

In April 2023, the South China Sea (SCS) experienced an unprecedented surge in aerosol loading, reaching the highest levels recorded in the two-decade Moderate Resolution Imaging Spectroradiometer (MODIS) satellite data period (2003–2023). Satellite observations revealed a 150% increase in aerosol optical depth (AOD) from MODIS and a 50% rise in carbon monoxide (CO) at 700 and 500 hPa from Measurements Of Pollution In The Troposphere (MOPITT) over SCS. Here, we investigate the drivers and atmospheric mechanisms responsible for this extreme event, identifying large-scale biomass burning (BB) across northern Peninsular Southeast Asia (PSEA), particularly Laos and Myanmar as the primary source. Our analysis indicates that anomalously high surface temperatures, low soil moisture, reduced precipitation, and a persistent upper-tropospheric anticyclone created favorable BB conditions over PSEA. Laos alone accounted for ~56% of the BB activity in the region, recording its largest monthly burned area (1.08 million hectares) since 2002. Dynamical analysis of the large-scale atmospheric circulation patterns revealed a major shift in regional wind regimes: the climatological south-westerlies over the SCS were replaced by anomalous northerlies, driven by the eastward shift of the Bay of Bengal anticyclone and the development of a cyclone anomaly over the western North Pacific (WNP). These changes redirected smoke transport from the usual WNP pathway to the SCS, resulting in significant transboundary pollution. This study highlights the critical role of compound meteorological extremes and circulation anomalies in amplifying regional aerosol loading, with implications for air quality, climate feedbacks, and environmental monitoring across Southeast Asia.

Key words: Aerosol loading; South China Sea; MODIS; Wildfires

1. Introduction

In the changing climate scenario, both natural and anthropogenic activities have contributed to a continuous increase in surface temperatures worldwide over the past decade (Seneviratne et al., 2021). In 2023, a record-high global mean surface temperature was observed, marking the warmest period in the last seven months (June to December), surpassing the previous record set in 2016 by a significant margin of 0.13°C to 0.17°C (Esper et al., 2024; Forster et al., 2024; Min, 2024; Raghuraman et al., 2024). The extreme temperatures contributed to record-breaking wildfires worldwide in 2023, with 70% of the total burning occurring in the Northern Hemisphere (Kolden et al., 2024). Among all, Canadian wildfires emerged as the primary hotspot in 2023, with significant fires in both the eastern and western regions causing notable increases in carbon monoxide (CO) and tropospheric aerosols over the past twenty years (Liu et al., 2024). The unprecedented wildfire season in Canada from May to September 2023 burned three times more biomass than the previous record, leading to the highest annual carbon emissions from biomass burning (BB) since 2015 (Byrne et al., 2024; MacCarthy et al., 2024). Furthermore, catastrophic wildfires have also occurred in regions such as Hawaii, the Mediterranean, central Amazonia, and central Chile (Roy et al., 2024; Lemus- Canovas et al., 2024; Espinoza et al., 2024; Jones et al., 2024; Cordero et al., 2024). Greece experienced its most severe wildfire on record, with a burned area of 96,000 hectares in 2023 (Michailidis et al., 2024). The August 2023 wildfires on Maui, Hawaii, were among the deadliest U.S. wildfire incidents, resulting in 100 deaths and an estimated loss of $5.5 billion (NOAA NCE, 2023). As a result of multiple fire spots across the globe, the global mean concentrations of atmospheric carbon dioxide (CO_2), methane (CH_4), and nitrous oxide (N_2O) reached new annual record highs of 419.3 ppm, 1922.6 ppb, and 336.7 ppb, respectively. The global atmospheric CO_2 growth rate in 2023 was 2.79 ± 0.08 ppm (Ke et al., 2024; Gui et al., 2024), the third-largest since 2000 and the fourth-largest since 1959.

The Asian region frequently experiences forest fires and biomass-burning activities, significantly impacting the global carbon footprint (Xia et al., 2025). The South China Sea (SCS) in Asia is the largest marginal ocean region in the tropical–subtropical western North Pacific. It is a prime example of a marine area with minimal air pollution (Pani et al., 2023). This is further supported by long-term satellite-measured Aerosol Optical Depth (AOD) spatial distribution. **Sup. Figures 1a** and **1b** indicate shallow AOD values with minimal standard deviations in the SCS, illustrating a clean marine environment. The SCS has a monsoon climate characterized by a northeast monsoon during winter and spring and a southwest monsoon during summer and autumn (Cui et al., 2016). These monsoon circulations allow natural and anthropogenic pollutants from East Asia to be lifted and transported over long distances to the SCS (Lin et al., 2013). During the summer monsoon season (August and September), the frequent burning of peat forests on the Maritime Continent (MC) also affects the adjacent regions of the southern SCS. In addition to East Asia and the MC, the springtime open biomass burning (BB) over Peninsular Southeast Asia (PSEA, including Myanmar, Thailand, Cambodia, Laos, and Vietnam) also impacts the SCS. The PSEA is one of the hotspot regions with the most intensive biomass-burning activities in the world (Lin et al., 2013; Reid et al., 2013) and is a major contributor to carbon emissions and atmospheric aerosols during the springtime (March-April). Open BB occurs almost every year during spring in the PSEA due to slash-and-burn agricultural activities (Lee et al., 2016; Tsay et al., 2016; Huang et al., 2020), emitting a substantial number of aerosols and trace gases into the atmosphere (Ou-Yang et al., 2022). The influence of aerosol loading over the SCS is strongly associated with the sources of aerosols and the prevailing wind circulation.

Although the unprecedented Canadian wildfires in 2023 garnered immense scientific interest and were well-documented in several studies, the record-breaking aerosol loading in the SCS in April 2023 received relatively little international attention. The historic event over the SCS in April 2023 can be observed from the Moderate Resolution Imaging Spectroradiometer (MODIS) Aqua AOD anomalies compared to the long-term mean (2003-2022), which shows extreme positive anomalies over the SCS and surrounding regions in April 2023, in contrast to the rest of the globe (**Fig. 1**). However, AOD anomalies in May further illustrate the absence of positive anomalies over the SCS and the presence of higher positive anomalies specifically over North America, particularly Canada. The time series of monthly mean AOD over the SCS further indicates a record-high AOD in April 2023 compared to the rest of the MODIS data from 2003 to 2023 (**Sup. Fig. 2d**). The exceptional record-breaking aerosol loading in April 2023 is unusual for remote marine locations such as the SCS and requires detailed investigation. In this communication, we examine the factors and physical processes that contributed to the unprecedented aerosol levels observed in April 2023, utilizing extensive data collected from multiple sources over an extended period. The following three major topics are explored in detail in the present study:

https://doi.org/10.5194/egusphere-2025-4223
Preprint. Discussion started: 4 September 2025

- How extreme are these AOD/CO anomalies, and what magnitude was increased?
- What are the sources for these record-breaking aerosol loadings over SCS?
- Were dynamic and large-scale circulations responsible for this event?

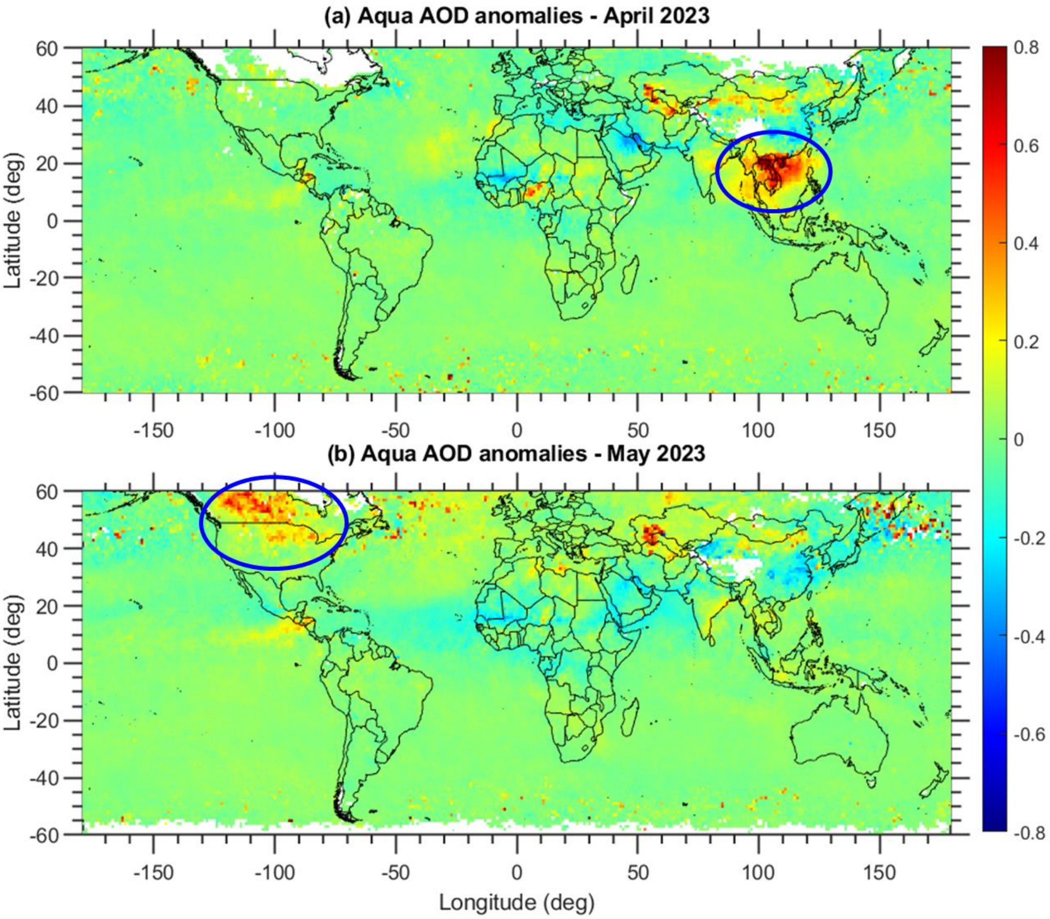

Figure 1. MODIS Aqua measured AOD anomalies in (a) April 2023 and (b) May 2023 compared to the long-term mean (2003-2022). The highlighted circles in (a) and (b) indicate the AOD anomalies over the South China Sea (SCS) and Canada regions. This figure highlights that the AOD anomalies observed by MODIS are significant and particularly pronounced over the SCS compared to the other areas globally. It illustrates the unique characteristics of April 2023 in terms of climatology. Data visualizations produced using MATLAB 2023b (https://matlab.mathworks.com).

2. Data and Methodology

2.1.1 Data

This study relies entirely on publicly available data, covering the period from 2003 to 2023. We used data products from various satellite measurements. For example, AOD data is obtained from MODIS, while CO data is obtained from MOPITT and AIRS satellites, respectively. The tropospheric column ozone data are obtained from OMI/MLS along with AIRS ozone data at 700 hPa and 500 hPa, respectively.

Moderate Resolution Imaging Spectroradiometer (MODIS)

MODIS is a passive sensor aboard the Aqua and Terra satellites, which are in a sun-synchronous orbit, and pass the Equator in the morning (Aqua) and afternoon (Terra). From MODIS satellite measurements, we utilized aerosol optical depth (AOD), fire counts, fire radiative power (FRP), cloud fraction, and burned area products. We used Level 3 monthly AOD at 1∘ × 1∘ spatial resolution derived from the mean of the Dark Target and Deep Blue Combined Aerosol Products from the Terra satellite (MOD08_M3 Collection 6.1) and Aqua satellite (MYD08_M3 Collection 6.1) (Platnick et al., 2015; Buchholz et al., 2020). Additionally, we utilized MODIS's product of daily fire counts and fire radiative power (FRP) (Giglio et al., 2006, 2016, 2018). Direct fire counts from MODIS were obtained from the Fire Information for Resource Management System (FIRMS) dataset. We selected all MODIS fire counts from the Terra and Aqua sensors with a confidence level of 80% or higher. Each month, the total MODIS daily fire counts and FRP are constructed and gridded at a resolution of 0.25° latitude × 0.25° longitude. Finally, we utilized Cloud Fraction data from both the Terra and Aqua satellites.

Measurements Of Pollution In The Troposphere (MOPITT)

MOPITT is a multi-channel thermal infrared (TIR) and near-infrared (NIR) instrument operating on board the sun-synchronous polar-orbiting NASA Terra satellite. This study uses a version 9 (MOP03TM_9) gridded monthly product (Worden et al., 2010; Deeter et al., 2019). For more details about the retrieval algorithm, validation, and uncertainties in MOPITT CO, refer to Deeter et al. (2019).

Atmospheric Infrared Sounder (AIRS)

https://doi.org/10.5194/egusphere-2025-4223
Preprint. Discussion started: 4 September 2025

In addition to the MOPITT measurements, we utilized CO from the AIRS on the NASA Aqua satellite, which provides CO at different vertical levels twice daily and has near-global coverage. AIRS uses wavenumbers 2183–2200 cm−1 (4.58–4.5 µm) for retrieving CO (McMillan et al., 2005). The V9 level 3 CO product, available at 1∘ × 1∘ resolution at various pressure levels, was utilized in the present study. AIRS sensitivity to CO is broad and optimal in the mid-troposphere between approximately 300 and 600 hPa (Warner et al., 2007, 2013; AIRS project, 2019). CO retrievals exhibit a 6%–10 % bias between 900 and 300 hPa with a root mean square error of 8%–12 % (McMillan et al., 2011). In addition to CO, we also utilized ozone, skin temperature, and outgoing longwave radiation (OLR) data from the AIRS satellite.

Ozone Monitoring Instrument (OMI)/Microwave Limb Sounder (MLS)

We utilized the OMI/MLS dataset of global tropospheric column ozone (TCO) concentrations, covering the period from 2005 to 2023, obtained from the Ozone Monitoring Instrument (OMI) and the Microwave Limb Sounder (MLS) (Ziemke et al., 2006). The total ozone column from OMI is derived using the Total Ozone Mapping Spectrometer (TOMS) version 8 algorithm. MLS measures vertical ozone profiles above the upper troposphere via limb scans ahead of the Aura satellite. TCO is then determined by subtracting MLS's stratospheric ozone measurements from OMI's total column ozone, after calibration adjustments between the two instruments via the convective-cloud differential method (Ziemke et al., 2006). The OMI/MLS product provides monthly mean TCO data between 60°S and 60°N at a 1° × 1° resolution, starting from October 2004. This dataset has been extensively used to analyze global tropospheric ozone patterns (Ziemke et al., 2019; Cooper et al., 2010) and long-term trends (Gaudel et al., 2018; Lu et al., 2019).

MERRA-2 reanalysis products

We also utilized monthly mean geopotential height, wind vectors (zonal and meridional wind speed), total column black carbon, organic carbon, and particulate matter from the Modern-Era Retrospective Analysis for Research and Applications, version 2 (MERRA-2). MERRA-2 is the latest atmospheric reanalysis data produced by the NASA Global Modeling and Assimilation Office (GMAO; Gelaro et al., 2017). The horizontal resolution of the MERRA-2 reanalysis is 0.5° × 0.625°.

Soil Moisture

Monthly mean soil moisture content (10 - 40 cm underground) from the Global Land Data Assimilation System (GLDAS)_NOAH025_M v2.1 is utilized. The data can be downloaded from https://hydro1.gesdisc.eosdis.nasa.gov/data/GLDAS/GLDAS_NOAH025_M.2.1/ (last accessed: June 05, 2025).

Precipitation

The Global Precipitation Climatology Project (GPCP) Version 3.2 Satellite-Gauge (SG) Combined Precipitation Data Set was used during the study period. The data is available for download from https://measures.gesdisc.eosdis.nasa.gov/data/GPCP/GPCPMON.3.2/ (last accessed June 5, 2025).

2.1.2 Methodology

The anomalies in the various parameters for April 2023 were estimated by subtracting the background long-term mean for April (2003-2022) from the value for April 2023.

The magnitude of the AOD/CO enhancement in April 2023 above the long-term background was determined by comparing the average of April 2003-2022. We obtained the percentage change in AOD/CO relative to the respective background using Equation 1:

$$\text{Relative change in percentage} = \left(\frac{x_{i-\bar{x}}}{\bar{x}}\right) \times 100 \qquad \text{(Eq. 1)}$$

where x_i represents the monthly mean of April in 2023, and $\bar{x}$ is the long-term mean of April calculated using the data from 2003 to 2022.

3. Results and Discussion

3.1 Record-breaking AOD and CO anomalies over SCS in April 2023

Aerosol optical depth (AOD) is a standard measure used to estimate aerosol loading and is a key parameter in calculating radiative effects. We utilize AOD data from MODIS instruments on the Aqua and Terra satellites from 2003 to 2023. **Sup. Figures 2a** and **2b** show the long-term (2003-2022) average AOD for April and the monthly mean AOD for April 2023. Time series of average monthly AOD values over northern PSEA (17-23 N, 99-106 E) and SCS (109-119 E, 11-18 N) from 2003 to 2023 are shown in **Sup—Figures 2c** and **2d**.

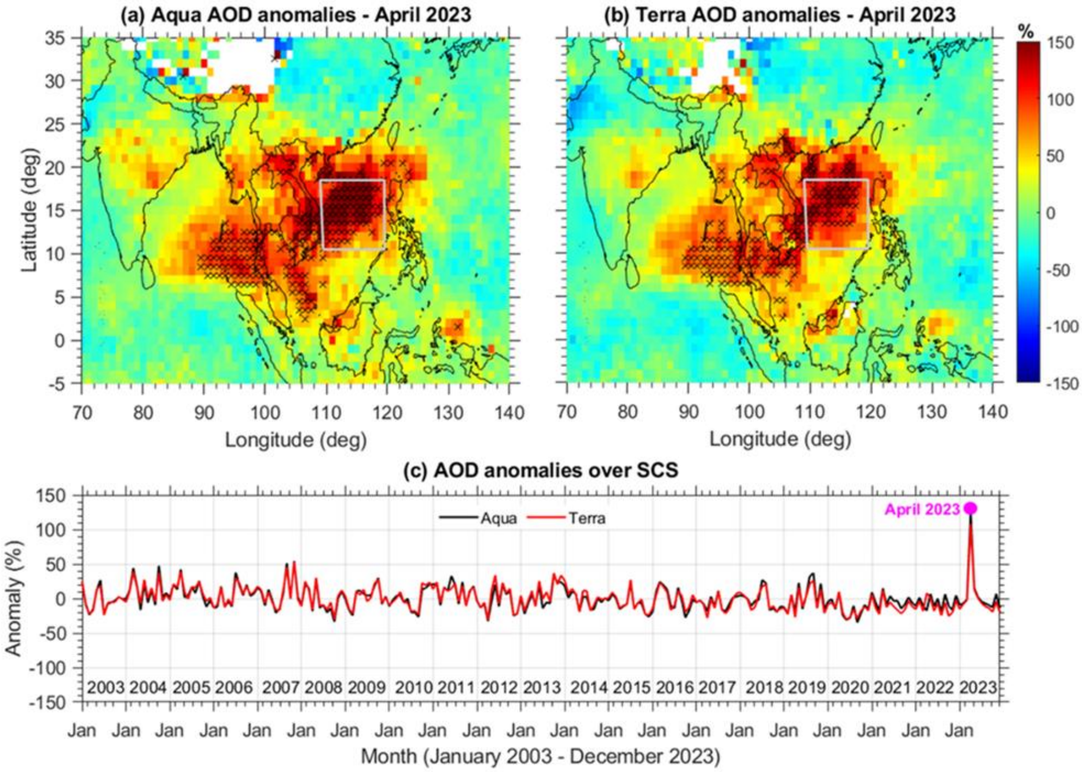

Figure 2. Spatial distribution of the change (%) in April 2023 Aerosol Optical Depth (AOD) values compared with the inter-annual April average (2003-2022). (a) AOD anomalies are obtained from the MODIS Aqua and (b) from the MODIS Terra satellite. The black hatches indicate that the anomalies exceed 4σ standard deviations of the long-term mean. (c) Time series of area-averaged AOD anomalies expressed in percentage change over the South China Sea (SCS) domain from the Aqua (black line) and Terra (red line) satellites. The most significant enhancement was in SCS, where the April AOD anomalies fell more than 4σ standard deviations.

The AOD distribution in April over two decades indicates high aerosol loading from northern Laos to coastal South China (15-25 N, 100-120 E). In April 2023, extreme AOD values extended from PSEA to South China and SCS, with the highest center between northern Laos and the SCS. Record-breaking AOD levels were observed for the area averaged over the SCS in April 2023, showing a nominal increase in northern PSEA (**Sup. Fig. 2c-d**). The highest AOD value for northern PSEA in April 2023 correlates with record AOD over the SCS. To assess the magnitude of the increase, we estimated the percentage change in AOD by comparing April 2023 with the

https://doi.org/10.5194/egusphere-2025-4223
Preprint. Discussion started: 4 September 2025

long-term average for April from 2003 to 2022. **Figures 2a** and **2b** depict the spatial extent of AOD anomalies expressed as percentage changes from MODIS Aqua and Terra. A surprising and widespread enhancement, with an increase of over 150% in most of the SCS and the southern Bay of Bengal (BoB), was evident in April 2023, and the increased anomalies exceeded approximately four standard deviation units. The area-averaged AOD anomalies (%) over the SCS domain from Aqua (black line) and Terra (red line) satellites show that the increase in April 2023 was a record high compared to MODIS data from 2003 to 2023, highlighting the extremity of AOD enhancement in that month. Satellite observations were further corroborated by ground-based in situ measurements from the AErosol RObotic NETwork (AERONET). The only operational AERONET remote station downwind of PSEA biomass burning, with over a decade of continuous AOD measurements (**Sup. Fig. 3a**), within the SCS region is located on Dongsha Island (also known as Pratas Island, 20.70°N, 116.73°E; 5 m a.s.l.). Analysis of the monthly mean AOD data from Dongsha Island indicates that April 2023 recorded the highest AOD value in the entire observational period from January 2009 to December 2023 (**Sup. Fig. 3c**).

We further investigated CO changes in April 2023 across the study region using MOPITT and AIRS satellite measurements, which provide over two decades of continuous CO data. CO is a crucial trace gas due to its role as a tropospheric pollutant, atmospheric transport tracer, and involvement in tropospheric chemistry. We analyzed CO data at 700 and 500 hPa from both satellites between 2003 and 2023. The 500 hPa level is the most sensitive altitude for CO measurements (Buchholz et al., 2021). The observed CO anomalies from the two satellites are shown in **Figure 3**, highlighting significantly elevated CO levels in April 2023 over the SCS, with increases up to 3σ standard deviations compared to the climatology from 2003 to 2022. Both instruments reveal distinct spatial anomalies, with MOPITT displaying more concentrated CO anomalies than AIRS. However, both show positive CO anomalies at both levels, indicating a significant increase in CO in April 2023. It is worth noting that the spatial distribution of CO anomalies aligns closely with AOD anomalies (**Fig. 2**). The area-averaged anomalies of AOD and 500 hPa CO over the SCS from 2003 to 2023 revealed a significant positive correlation of approximately 0.65 (**Sup. Figure 4**). This strong correlation in April (2003–2023) suggests that long-range pollution transport likely drives AOD variability in this region during April. The bubble chart illustrates the severity of April 2023 compared to other years over the SCS (**Sup. Figure 4**). CO production from incomplete combustion indicates that elevated levels far from traffic or industrial sources suggest biomass burning and wildfire emissions. This implies smoke transport from surrounding regions to the SCS and the BoB, near significant BB hotspots, including the MC and PSEA. **Sup. Figure 1c-1d** shows annual AOD fluctuations, with peaks in April over PSEA and September over MC. The MC's fire season is from August to October, while PSEA experiences a BB season from January to April, peaking in March. This strongly suggested that the high AOD levels in April 2023 over the SCS were linked to BB activities in PSEA.

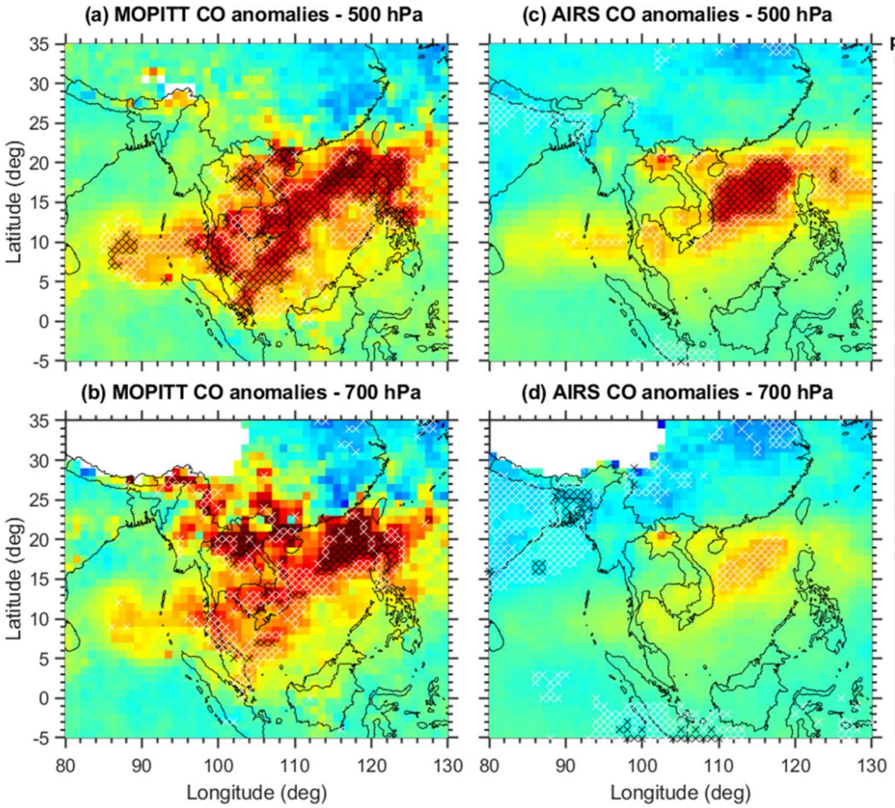

Figure 3. Spatial distribution of carbon monoxide anomalies in April 2023 at (a) 500 hPa and (b) 700 hPa obtained from MOPITT satellite measurements. Subplots (c) and (d) are identical to subplots (a) and (b), but the results are obtained from AIRS satellite measurements. The anomalies compared to the long-term mean of April from 2003 to 2022. The black and white hatches indicate that the anomalies are more significant than 3σ and 2σ standard deviations, respectively.

3.2 Biomass Burning activity over PSEA in April 2023

We further examined BB activity over PSEA in April 2023, using MODIS fire counts and fire radiative power (FRP) as proxies for BB activities and wildfires. It is noted that there were a total of 21198 fire counts and a total FRP of 2407283 (MW) throughout PSEA (**Sup. Table 1**). Fire counts and FRP varied significantly between countries, with Laos reporting the highest number of fire counts (11877) and FRP (1530000 MW). Notably, Laos accounted for 56% of the total fire counts and 63% of the FRP for PSEA, establishing it as a hotspot for BB activity in April 2023. **Figures 4a** and **b** show the spatial distribution of fire counts and the related FRP over PSEA in April 2023. Persistent and more intense fires were observed over northern Laos and Myanmar, with the most intense fires occurring north of Laos. The number of fires in Laos in April 2023 was the highest recorded in the past 20 years (**Fig. 4c**). It should be noted that Laos is characterized by around 60% of its land cover types being forests (**Sup. Fig. 5**). Most of this forest is situated in northern Laos, where most fires occurred in April 2023. This suggests that forest fires in Laos were primarily responsible for the majority of fires in 2023. Although the FRP in 2023 was not at its peak, it was still among the highest BB activities, following 2016 and 2003. However, the nighttime fires and corresponding FRP demonstrate that the 2023 BB activity was the highest in the entire MODIS data record and exceptionally intense in terms of FRP (**Figs. 4e-4f**). This demonstrated the intensity of the fires in April 2023 compared to the last 20 years. The extreme nighttime fire activity highlights changes in fire behavior and environmental or human factors that favored intense nighttime burning in April 2023. We further examined area-averaged fires and FRP over northern Laos (17-23^{o}N), indicating that the highest fires and FRP were recorded in April 2023 in MODIS data from January 2003 to December 2023 (**Sup. Fig. 6**). Furthermore, the MODIS estimated monthly burned area product (MCD64A1) reveals a total area of 1.08 million hectares burned in Laos in April 2023, the highest monthly value in the available data for that dataset (2002–2023; **Sup. Fig. 7**). The spatial distribution of the MODIS burned area (**Sup. Fig. 8a**) shows that the most significant area affected by fires in 2023 was located in northern Laos, which closely aligns with the total number of fires and the FRP illustrated in **Figure 4**. This raises the question: What caused the anomalous fire activity in Laos in April 2023? We examined various meteorological and dynamic conditions in April 2023 to address this.

https://doi.org/10.5194/egusphere-2025-4223
Preprint. Discussion started: 4 September 2025

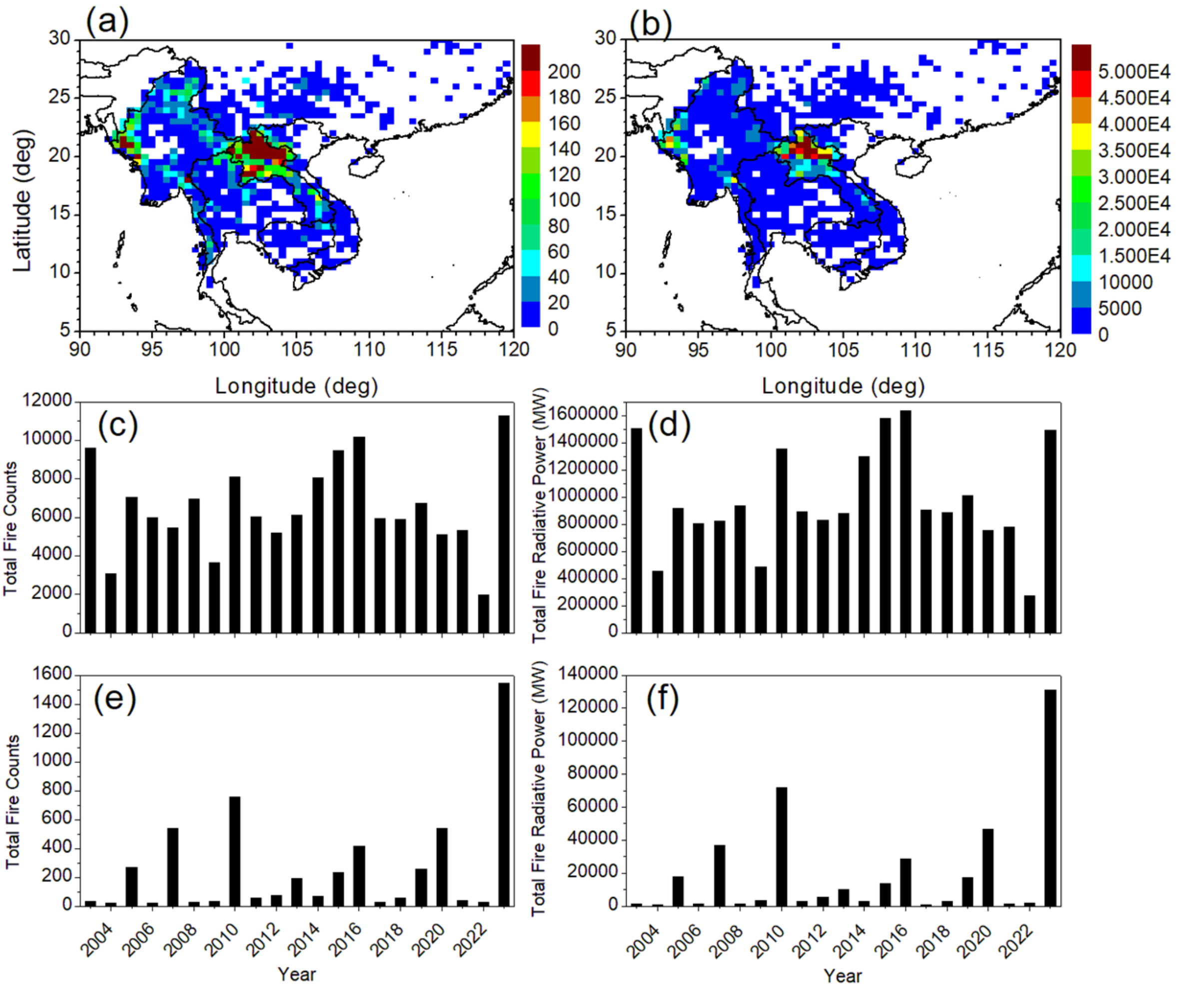

Figure 4. Spatial distribution (0.25° × 0.25°) of MODIS (a) fire counts and (b) total fire radiative power (FRP) in April 2023. A notable increase in fire activity over northern Laos is observed. (c) Inter-annual (2003 to 2023) monthly fire counts (day and night), and (d) the total FRP for April over Laos. (e) Inter-annual monthly nighttime fire counts and (f) the total FRP for nighttime fire counts over Laos in April. Fires with a confidence level of more than 80% are considered for the present analysis.

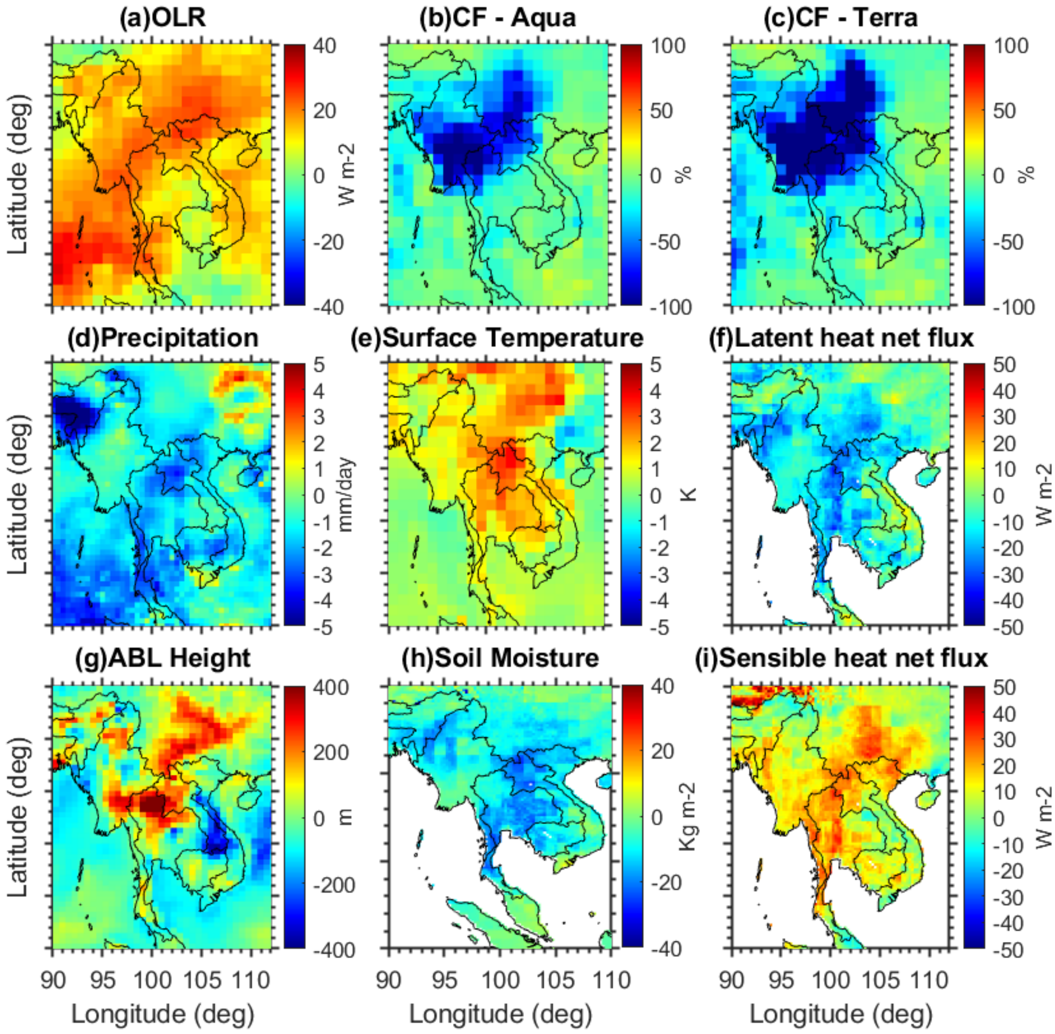

Figure 5. Surface and atmosphere conditions in April 2023. April anomalies in 2023 compared to the 2003-2022 climatological period for (a) Outgoing Longwave radiation (OLR), (b) cloud fraction (CF) from Aqua, (c) cloud fraction from Terra, (d) precipitation, (e) Surface Temperature, (f) surface latent heat flux, (g) Atmospheric Boundary Layer (ABL) Height, (h) soil moisture (10 - 40 cm underground), and (i) surface sensible heat flux. OLR and surface temperatures are obtained from AIRS satellite measurements. CF data from MODIS Aqua and Terra. ABL height obtained from MERRA-2 reanalysis. Soil moisture, surface latent heat, and sensible heat flux are obtained from the GLDAS Noah Land Surface Model L4 monthly 0.25 x 0.25 degree V2.1. Precipitation data is obtained from the Global Precipitation Climatology Project (GPCP) Version 3.2.

In April 2023, Outgoing Longwave Radiation (OLR) anomalies reflected decreased convective activity over PSEA, resulting in reduced precipitation, higher temperatures, and low

https://doi.org/10.5194/egusphere-2025-4223
Preprint. Discussion started: 4 September 2025

soil moisture (SM), as shown in **Fig. 5**. Precipitation, temperature, and SM anomalies correlate with enhanced MODIS fire counts and FRP over northern Laos (**Fig. 4**). Long-term SM anomalies in northern Laos reached record lows in April 2023, the lowest in two decades (**Sup. Figs. 9a and b**). We further examined the evolution of SM anomalies during 2021-2023, which indicates maximum positive values in March 2022 and maximum negative anomalies in April 2023, signifying prolonged drought from winter 2022 to April 2023 (**Sup. Fig. 9c**). Interestingly, the record-low SM anomalies occurred during the transition period from La Niña to El Niño. Under dry conditions, increased sensible heat flux warms the near-surface atmosphere, resulting in a positive land-atmosphere feedback (Alexander 2011). To explore how record SM anomalies in April 2023 affected land-atmospheric coupling, we analyzed surface heat flux changes over PSEA, revealing decreased surface latent heat flux and increased sensible heat flux. The negative latent heat flux anomalies indicated limited evapotranspiration due to dry soil conditions. A deeper Atmospheric Boundary Layer (ABL) height (>400 m increase) was observed over northern PSEA, particularly in Laos, aligning with other anomalies in April 2023. Negative SM anomalies favor a positive geopotential height anomaly in upper levels, maintaining local high pressure and promoting surface warming (Fischer et al., 2007; Dong et al., 2023). The northern PSEA experienced a high-pressure anticyclone in April 2023 (**Fig. 6a**), which decreased cloud cover, increased solar radiation and surface temperature, and reduced precipitation. MODIS cloud fraction (CF) anomalies exhibited extreme negative values, particularly in the northern PSEA, decreasing by over 100% compared to the 2003-2022 average, closely aligning with the high-pressure anticyclone depicted in **Figure 6a**. Reduced cloud cover and drier soil will increase heat, landscape flammability, and wildfire potential. It is concluded that record-breaking negative SM anomalies under a deeper, drier, and warmer ABL, coupled with increased temperatures, low precipitation, and anomalous low cloud cover associated with the upper tropospheric high-pressure system, contributed to record-breaking BB and wildfires over Laos in April 2023.

3.3 Dynamical and large-scale circulations in April 2023

Previous research shows that in spring, smoke aerosols (BC and OC) and trace gases are transported from PSEA to downstream areas like southern SC, Taiwan, and the northwestern Pacific via free tropospheric westerlies (Wai et al., 2008; Lin et al., 2009; Lin et al., 2013; Yen et al., 2013; Chuang et al., 2014; Ou-Yang et al., 2014; Lin et al., 2017; Pani et al., 2019).

Remarkably, in April 2023, PSEA BB smoke aerosols and trace gases were transported to the far southern regions of the SCS and the BoB, marking a significant departure from the usual transport pathway to downwind Taiwan and the northwest Pacific, respectively.

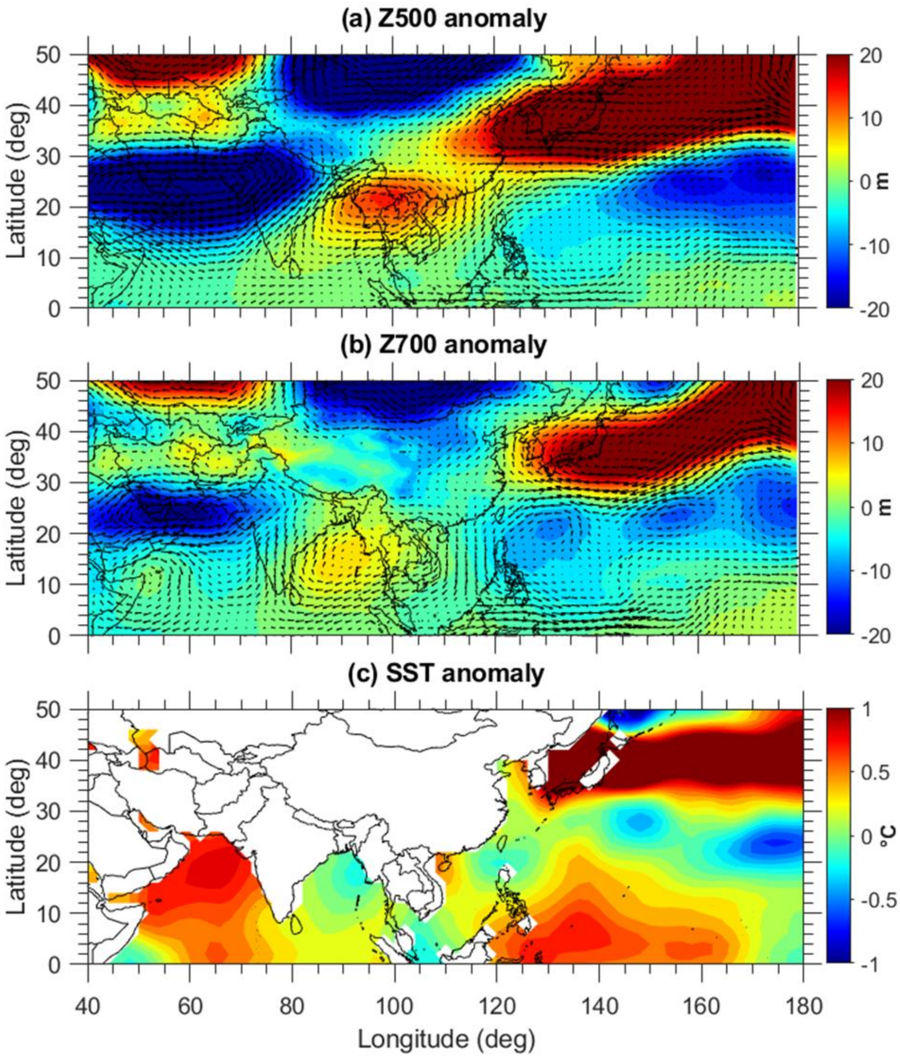

Figure 6. Spatial distribution of (a) 500 hPa geopotential height (Z500), (b) 700 hPa geopotential height (Z700), and (c) Sea Surface Temperature (SST) anomalies in April 2023. The anomalies are calculated by subtracting the monthly mean of April 2023 from the April climatology for the period from 1991 to 2020. The wind anomalies for the respective pressure levels are overlaid in Z500 and Z700 anomalies. The geopotential height and wind data are from the MERRA-2 reanalysis, while SST data are from the NOAA Extended Reconstructed SST V5.

Here, background dynamics and large-scale circulations are crucial for transporting smoke aerosols over longer distances from the sources (Ravindra Babu et al., 2023; Huang et al., 2024). To provide context for the April 2023 event, we briefly analyzed the large-scale circulation patterns responsible for the unprecedented aerosol loading. Our focus was on the geopotential height and winds, both zonal and meridional, at 700 and 500 hPa levels. The geopotential height observed at these levels (Z700 and Z500) in April 2023 contrasts with the background climatology of April (1991-2020) (**Sup. Figs. 10 and 11**). Specifically, at 700 hPa (Z700), a high-pressure system over the Indian region shifted eastward, reaching the PSEA. In comparison, at 500 hPa (Z500), the western Pacific anticyclone shifted westward to sit directly above the PSEA. To get a clearer picture, we further obtained the anomaly in Z700 and Z500 in April 2023 by comparing the long-term mean of 1991-2020. The observed Z700 and Z500 anomaly composites are illustrated in **Figure 6a and b**. There is a prominent anomalous anticyclone over northern PSEA, centered roughly at 20°N, 100°E (**Fig. 6a**). Additionally, a significant anomalous low-level cyclone is present over the western North Pacific (WNP) around the Philippines, with an anomalous cyclone forming upstream and downstream of the anticyclone over the PSEA, creating a zonal low-high-low (L-H-L) pattern. This arrangement might suggest the movement of a Rossby wave train (Hu et al., 2024). Concurrently, a strong anticyclone anomaly was situated over the northern Pacific Ocean, just above the western Pacific cyclone anomaly. It is strongly indicated from **Figures 5** and **6** that the upper- and lower-level anomalous anticyclones significantly caused cloudless skies, reduced precipitation, and elevated surface temperatures in the PSEA. These favorable conditions, occurring over drier soil, led to extreme BB and wildfires in Laos, which released significant quantities of aerosols and trace gases into the atmosphere.

We hypothesize that these systems, including an anomalous WNP cyclone, a BoB anticyclone at 700 hPa, and a high-pressure anticyclone over PSEA at 500 hPa, substantially influenced the background circulations in the PSEA and its surroundings. This interaction likely contributed to the unusual BB smoke transport from northern PSEA to the SCS and the BoB in April 2023, as corroborated by the meridional wind anomalies in **Sup**. **Figs. 12b and c**, which indicate unusual northerly winds over the SCS. The northerly wind anomalies inhibited smoke transport from northern PSEA to the SCS, resulting in unprecedented aerosol loading over the SCS and the BoB. Additionally, zonal wind anomalies showed typical background westerlies supplanted by easterlies over the North Pacific near Japan, due to an anomalous high-pressure

https://doi.org/10.5194/egusphere-2025-4223
Preprint. Discussion started: 4 September 2025

system in April 2023 (**Sup. Figs. 12a and b**). This high-pressure system weakened the westerlies to its south, obstructing the usual smoke transport from PSEA to the downwind northwestern Pacific. This is further supported by AERONET observations from Lulin Atmospheric Background Station (LABS, 23°28′N, 120°52′E, 2,862 m; Sheu et al., 2010), located downwind of the PSEA smoke (**Sup. Fig. 12a**). The AOD data revealed no notable rise in AOD at Lulin in April 2023 compared to previous years, similar to what was observed at Dongsha Island (**Sup. Fig. 13c**). In conclusion, the unusual circulation from the BoB anticyclone and the WNP cyclone transported PSEA smoke into the SCS, resulting in unprecedented aerosol loading in April 2023. Exploring the causes and dynamics behind the anti-cyclonic and cyclonic circulations over the BoB and WNP in April 2023 is intriguing; however, it falls outside the scope of this study. Preliminary analysis of sea surface temperature (SST) anomalies in April 2023 revealed a distinct and spatially coherent pattern across the Pacific Ocean (**Fig. 6c**). Notably, positive SST anomalies were observed over the western Pacific warm pool near the equatorial region, while negative anomalies appeared over the central to eastern equatorial Pacific. In addition, strong positive SST anomalies were present over the mid-latitude North Pacific. This tri-polar SST structure is known to influence large-scale atmospheric circulation patterns. According to the Matsuno–Gill framework, enhanced warming in the tropical western Pacific can induce anomalous cyclonic circulation over the WNP (Gill, 1980; Zeng and Sun, 2022). Concurrently, regional SST anomalies over the Indian Ocean exhibited positive values in the Arabian Sea and negative anomalies in the BoB. These SST anomalies corresponded closely with 700 hPa geopotential height (Z700) anomalies, which were positive over the BoB and negative over the Arabian Sea. The spatial alignment of SST and Z700 anomalies suggests that the observed SST anomaly configuration in April 2023 likely exerted a substantial influence on tropospheric circulation over both the Indian and Pacific Oceans.

3.4 Impact on Tropospheric Ozone

It is well known that BB smoke can emit aerosols and various gaseous compounds, including nitrogen oxides (NO_x), CO, methane (CH_4), and multiple volatile organic compounds (VOCs). Once emitted, BB smoke undergoes chemical transformations in the atmosphere, altering the mix of compounds and generating secondary pollutants such as ozone (O_3) and secondary organic aerosol (Jaffe and Wigder, 2012; Ogino et al., 2022). BB emissions from the PSEA have a significant impact on air quality and weather in both source and downwind regions. In previous sections, we demonstrated the record-breaking increase in AOD, along with the unusual enhancement in tropospheric CO (at 700 and 500 hPa) over SCS due to PSEA biomass burning. It is known that the presence of CO is one of the factors that control the abundance of tropospheric ozone, a short-lived pollutant and climate forcer (Liu et al., 1999; Chan et al., 2003; Ou-Yang et al., 2012; Yadav et al., 2017; Liao et al., 2021).

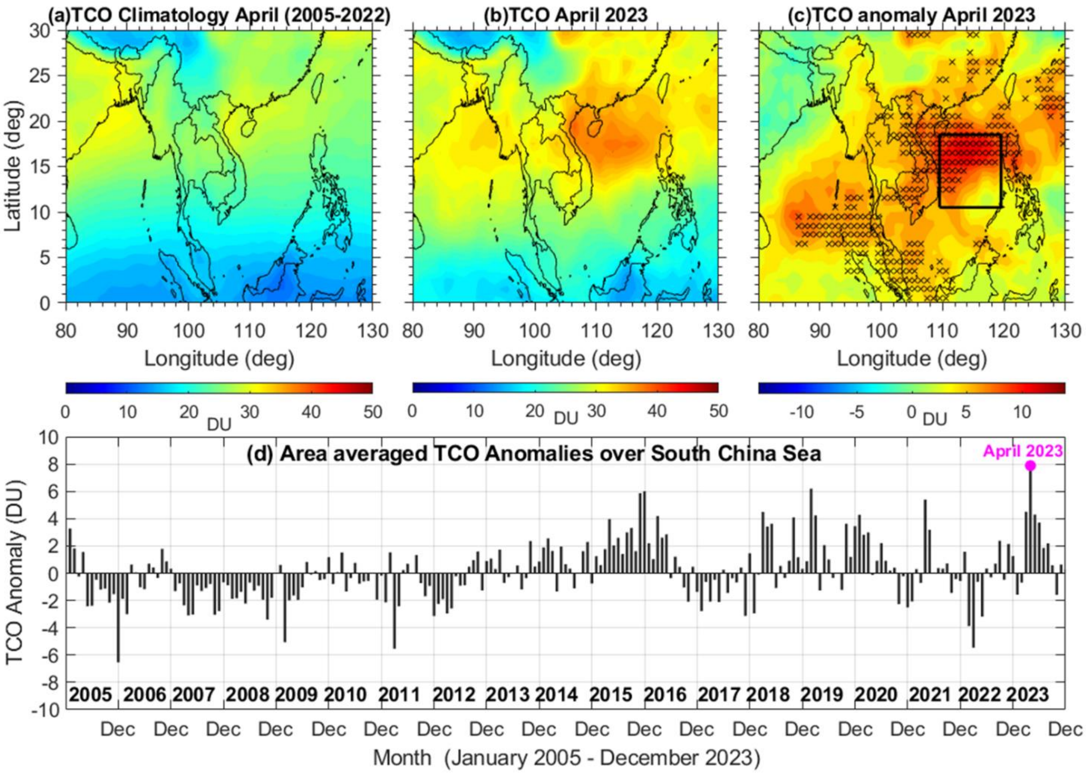

Figure 7. Spatial distribution of tropospheric column ozone (TCO) (surface - 300 hPa ozone column) concentrations in (a) April (2005-2022), (b) April 2023. (c). The observed spatial distribution of TCO anomaly in April 2023. Anomalies based on removing the 2005-2022 April mean. (d) The area-averaged TCO anomalies observed over SCS between January 2005 and December 2023—anomalies based on removing the long-term mean from 2005 to 2022. The highest increase in the TCO for the SCS region is recorded in April 2023 during the OMI/MLS data period. The black hatches in sub-plot (c) indicate that the anomalies are more significant than 3σ standard deviations, respectively.

Here, we investigated how this record-breaking pollution event may have influenced tropospheric ozone levels in April 2023. We analyzed long-term tropospheric ozone column (TOC) data (surface to 300 hPa) from the combined Aura Ozone Monitoring Instrument and Microwave Limb

https://doi.org/10.5194/egusphere-2025-4223
Preprint. Discussion started: 4 September 2025

Sounder satellite ozone measurements (OMI/MLS) from 2005 to 2023 (Ziemke et al., 2006; 2019). **Figures 7a** and **7b** illustrate the spatial distribution of the long-term April mean and the April 2023 TOC over the study area. Additionally, **Figure 7c** illustrates the observed anomaly in April 2023 in comparison to the long-term average. We also include area-averaged TOC anomalies over the SCS spanning the entire OMI/MLS dataset. The OMI/MLS TOC anomaly indicates significantly elevated ozone levels over the SCS and nearby regions during April 2023. The observed anomalies are statistically significant, being three standard deviations above the long-term mean of total column ozone (TOC). Furthermore, the monthly mean anomalies, averaged over the SCS throughout the entire OMI/MLS data period, reveal the highest increase in TOC, approximately 8 Dobson Units (DU), in April 2023. These exceptional TCO increases from the OMI/MLS data are further supported by the AIRS satellite O_3 measurements and the downwind ozonesonde measurements at Hong Kong, which are presented in **Sup. Figure 14**, respectively. We utilized long-term ozone measurements from the AIRS satellite from 2003 to 2023. Our analysis of 700 and 500 hPa levels reveals a substantial O_3 increase over SCS and nearby areas, about 20 ppb, exceeding two standard deviations of the long-term mean, corroborated by downwind Hong Kong ozonesonde measurements (**Sup. Figs. 14c and d**). The ozone profile peaks at altitudes of 3 to 4 km, with anomalies exceeding 30 ppb in the 3 to 5 km region, correlating exactly with the CALIPSO vertical aerosol enhancement. This illustrates the exceptional augmentation of TOC over the SCS in April 2023, comparable to the AOD increase observed in the MODIS data. Such findings are corroborated by the corresponding increases in CO levels recorded by MOPITT and AIRS at 700 hPa and 500 hPa, respectively, indicating a substantial influence of BB plumes originating from the PSEA region in 2023. Overall, the present analysis concludes that the April 2023 event had a significant impact on air quality over PSEA and its surrounding areas.

4. Summary and Conclusions

In April 2023, we observed an unprecedented increase in aerosol loading over the South China Sea (SCS), which had not been observed in the past two decades of the MODIS period, spanning from 2003 to 2023. Satellite observations revealed a 150% rise in aerosol optical depth (MODIS), alongside 50% increases in carbon monoxide (MOPITT) at 700 and 500 hPa over SCS. This study primarily focused on analyzing the drivers, physical and dynamical mechanisms behind the record-breaking aerosol loading over the SCS in April 2023. Our findings indicate that extreme biomass burning (BB) activity over northern PSEA was the primary source of the record-breaking aerosols in April 2023.

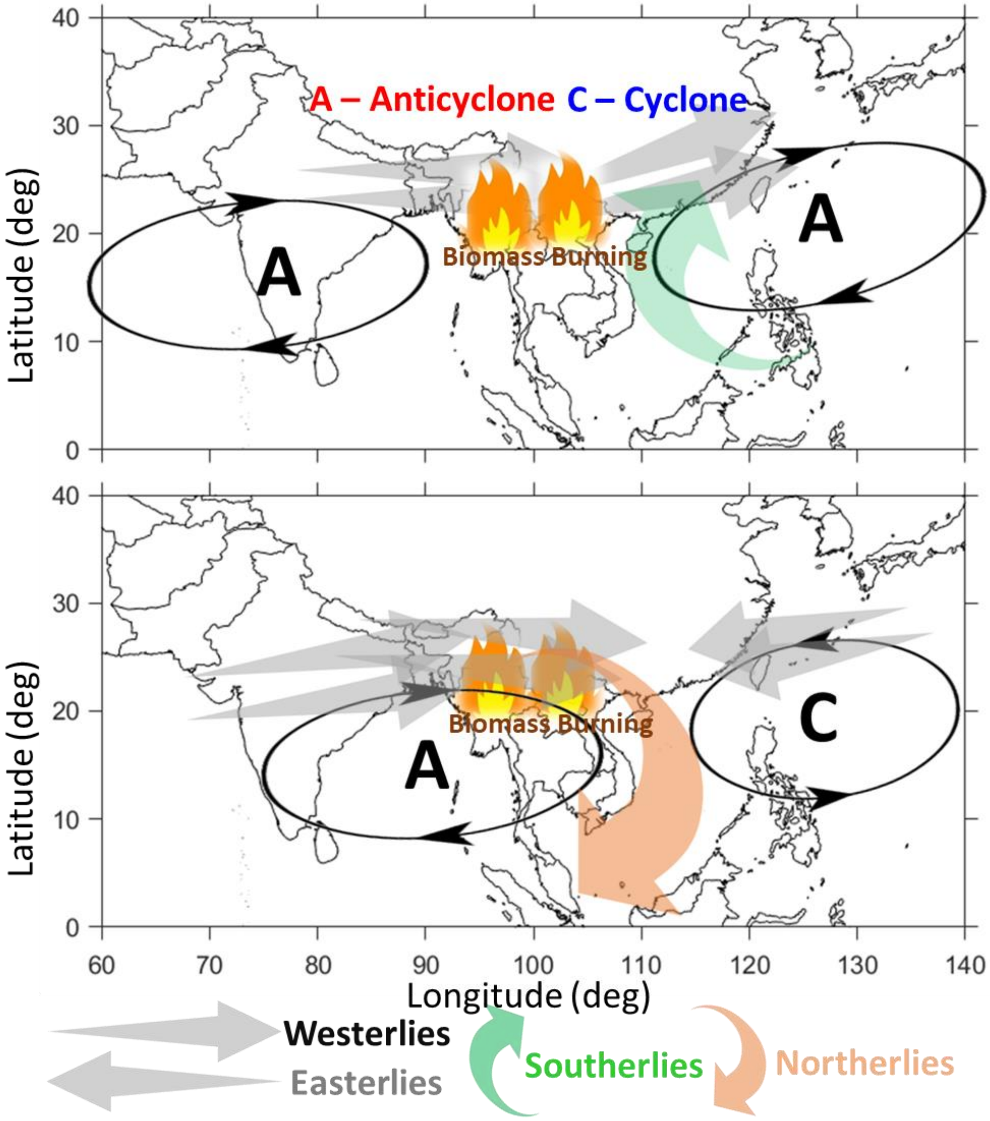

Figure 8. The schematic diagram illustrates the physical mechanisms responsible for the record-breaking aerosol loading over the South China Sea in April 2023. The top panel displays the long-term mean state in April, whereas the bottom panel shows the April 2023 mean state of the large-scale dynamical and circulatory systems. A denotes the presence of an anticyclone anomaly, and C represents the presence of a cyclone anomaly. The horizontal arrows indicate subtropical free-

tropospheric westerlies and easterlies. The green arrow indicates southerlies, and northerlies are shown by the brown arrow, respectively. Two anticyclone systems were present in climatology over the western Pacific and the Indian Ocean. Southwesterly and southerly winds in the free troposphere dominate the SCS. Free tropospheric westerlies transport smoke into the downwind areas of Taiwan and the western North Pacific. In April 2023, the western North Pacific anticyclone transitioned into an anomalous cyclone over the western North Pacific. The Indian anticyclone system further shifted eastward around the PSEA. Unusual northerly winds replaced the southerly winds due to a cyclone anomaly over the western North Pacific and an expanded Indian anticyclone. Additionally, in April 2023, easterlies around Taiwan and above hindered downwind transport to the northwestern Pacific.

An analysis of various meteorological and atmospheric factors reveals that the PSEA region has experienced unusual weather patterns, creating conditions conducive to BB and wildfires. Key contributors include extremely low soil moisture, higher surface temperatures, lower precipitation levels, and an upper tropospheric high-pressure anticyclone. These factors increase the likelihood of severe fire events, especially in Laos and Myanmar. Particularly, Laos became one of the hotspot regions for extreme BB activity in April 2023. Among all the countries in PSEA, Laos alone contributed approximately 56% of the total fire activity over PSEA, followed by Myanmar at around 33%. Under prolonged dry conditions, BB activity over Laos in April 2023 was higher than in the past two decades. The largest area burned, 1.08 million hectares, in a single month (2002-2023), occurred in April 2023. Additionally, unusually large-scale atmospheric circulations significantly spread smoke, trace gases, and pollutants to downwind regions from the source. Our analysis of large-scale circulations associated with dynamical changes illustrates the mechanism behind the April 2023 event, as schematically shown in **Figure 8**. In climatology, two anticyclone systems were situated over the WNP and the Indian Ocean. The SCS experiences predominantly southwesterly and southerly winds in the free troposphere. Westerly winds in the free troposphere generally transport BB smoke from PSEA to downwind areas of Taiwan and the WNP. In April 2023, the anticyclone over the WNP transformed into an unusual cyclone. Meanwhile, the Indian anticyclone shifted eastward over the BoB and near the PSEA. Due to a cyclone anomaly in the WNP and a persistent anticyclone in the BoB, northerly winds replaced the southerly winds in the free troposphere over the SCS. Additionally, in April 2023, easterlies near Taiwan obstructed downwind transport towards the northwestern Pacific. Overall, it is concluded that the regime shifted from southerlies to northerlies over the SCS due to the combined impact of the extended BoB anticyclone and the WNP cyclone, causing BB smoke transport from the PSEA to the SCS.

The present findings would benefit regional monitoring and a better understanding of the transboundary pollution over the PSEA.

Interestingly, PSEA is linked to an extreme heatwave in April 2023, with record-high temperatures (Zachariah et al., 2024; Lyu et al., 2024). Studies have attributed this heatwave to climate change (Zachariah et al., 2024), as well as to the strengthening of high pressure from tropical waves, moisture deficiency, and strong land-atmosphere coupling (Lyu et al., 2024). Our results further suggest a plausible role for BB-associated aerosols and greenhouse gases in the April 2023 heatwave. What role does heat trapping play in increasing greenhouse gases resulting from record-breaking BB activity? What is the impact of increased BB aerosols? Further research is needed to understand the exceptional conditions in PSEA and its surrounding regions, including BB-associated greenhouse gas emissions (GHGs) and aerosol anomalies. Additionally, smoke aerosols impact surface and atmospheric radiation budgets, affecting regional weather and climate. Future work will focus on the radiative energy balance and weather changes resulting from the April 2023 aerosol increase.

Data availability

MODIS data available from https://modis.gsfc.nasa.gov/data/dataprod/mod08.php. The AIRS and MOPITT CO data can be downloaded from https://disc.gsfc.nasa.gov/datasets/AIRS3STM_7.0 (AIRS project, 2019) and https://asdc.larc.nasa.gov/project/MOPITT/MOP02J_8 (NASA, 2023a). MERRA-2 data are available online through the NASA Goddard Earth Sciences Data Information Services Center (GES DISC; https://disc.gsfc.nasa.gov; NASA, 2023b). The MODIS fire products can be downloaded from https://firms.modaps.eosdis.nasa.gov/active_fire/ (NASA, 2023c). The OMI/MLS tropospheric column ozone data can be obtained from https://acd-ext.gsfc.nasa.gov/Data_services/cloud_slice/ (last access 01 July 2025).

Author Contributions

Saginela Ravindra Babu: Conceptualization, Data curation, Formal analysis, Investigation, Software, Validation, Visualization, Writing – original draft preparation, Writing – review and editing; **Neng-Huei Lin**: Conceptualization, Investigation, Funding Acquisition, Supervision, Resources, Writing – review and editing.

Competing interests

The authors declare no competing interests.

Acknowledgements

We acknowledge the National Science and Technology Council of Taiwan for supporting the research. The authors thank NASA and NOAA for providing MOPITT, MODIS, and AIRS satellite data. We thank NASA's Global Monitoring and Assimilation Office (GMAO) for providing the Modern-Era Retrospective analysis for Research and Applications, Version 2 (MERRA-2) data.

References

Seneviratne, S. I. et al. Weather and Climate Extreme Events in a Changing Climate. In Proc. Climate Change 2021: The Physical Science Basis. Contribution of Working Group I to the Sixth Assessment Report of the Intergovernmental Panel on Climate Change, 1513–1766 (Cambridge University Press, 2021). https://doi.org/10.1017/9781009157896.013.

Esper, J., Torbenson, M. & Büntgen, U. 2023 summer warmth unparalleled over the past 2,000 years. Nature 631, 94–97 (2024). https://doi.org/10.1038/s41586-024-07512-y

Forster, P. M. et al. Indicators of Global Climate Change 2023: annual update of key indicators of the state of the climate system and human influence. Earth Syst. Sci. Data 16, 2625–2658 (2024). https://doi.org/10.5194/essd-16-2625-2024

Min, S. K. Human influence can explain the widespread exceptional warmth in 2023. Commun. Earth Environ. 5, 215 (2024). https://doi.org/10.1038/s43247-024-01391-x

Perkins-Kirkpatrick, S., Barriopedro, D., Jha, R. et al. Extreme terrestrial heat in 2023. Nat Rev Earth Environ 5, 244–246 (2024). https://doi.org/10.1038/s43017-024-00536-y

Raghuraman, S. P. et al. The 2023 global warming spike was driven by the El Niño–Southern Oscillation. Atmos. Chem. Phys. 24, 11275–11283 (2024). https://doi.org/10.5194/acp-24-11275-2024

Kolden, C. A., Abatzoglou, J. T., Jones, M. W. & Jain, P. Wildfires in 2023. Nat. Rev. Earth Environ. 5, 238–240 (2024).

Liu, Z., Deng, Z., Davis, S. J. et al. Global carbon emissions in 2023. Nat. Rev. Earth Environ. 5, 253–254 (2024). https://doi.org/10.1038/s43017-024-00532-2

Byrne, B., Liu, J., Bowman, K. W. et al. Carbon emissions from the 2023 Canadian wildfires. Nature 633, 835–839 (2024). https://doi.org/10.1038/s41586-024-07878-z

MacCarthy, J., Tyukavina, A., Weisse, M. J., Harris, N. & Glen, E. Extreme wildfires in Canada and their contribution to global loss in tree cover and carbon emissions in 2023. Glob. Change Biol. 30, e17392 (2024). https://doi.org/10.1111/gcb.17392

Jain, P., Barber, Q.E., Taylor, S.W. et al. Drivers and Impacts of the Record Breaking 2023 Wildfire Season in Canada. Nature Commun. 15, 6764 (2024). https://doi.org/10.1038/s41467-024-51154-7

Lai, G. & Zhang Y. Increased atmospheric aridity and reduced precipitation drive the 2023 extreme wildfire season in Canada. Geophy. Res. Lett., 52, e2024GL114492 (2025). https://doi.org/10.1029/2024GL114492

Liu, G., Li, J. Li X. & Ying T. North Atlantic and the Barents Sea variability contribute to the 2023 extreme fire season in Canada. Proc. Natl Acad. Sci. USA, 121 (49) e2414241121 (2024). https://doi.org/10.1073/pnas.241424112

Roy, D. P., De Lemos, H., Huang, H., Giglio, L., Houborg, R. & Miura, T. Multi-resolution monitoring of the 2023 Maui wildfires, implications and needs for satellite-based wildfire disaster monitoring. Sci. Remote Sens. 10, 100142 (2024). https://doi.org/10.1016/j.srs.2024.100142

Lemus-Canovas, M., Insua-Costa, D., Trigo, R. M. & Miralles, D. G. Record-shattering 2023 Spring heatwave in western Mediterranean amplified by long-term drought. Npj Clim. Atmos. Sci. 7, 25 (2024). https://doi.org/10.1038/s41612-024-00569-6.

Espinoza, J.-C. et al. The new record of drought and warmth in the Amazon in 2023 related to regional and global climatic features. Sci. Rep. 14, 8107 (2024). https://doi.org/10.1038/s41598-024-58782-5

Jones, M. W. et al. State of wildfires 2023–2024. Earth Syst. Sci. Data 16, 3601–3685 (2024). https://doi.org/10.5194/essd-16-3601-2024

Cordero, R.R., Feron, S., Damiani, A. et al. Extreme fire weather in Chile driven by climate change and El Niño–Southern Oscillation (ENSO). Sci Rep 14, 1974 (2024). https://doi.org/10.1038/s41598-024-52481-x

Michailidis, K. et al. Extreme wildfires over northern Greece during summer 2023 – part A: Effects on aerosol optical properties and solar UV radiation. Atmos. Res. 311, 107700 (2024). https://doi.org/10.1016/j.atmosres.2024.

NOAA NCE, 2023. National oceanic and atmospheric administration (NOAA) national centers for environmental information (NCE), September 11th 2023. "U.S. Billion- dollar weather and climate disasters 1980-2023 report". Available online at: https:// www.ncei.noaa.gov/access/billions/events.pdf

Ke, P. et al. Low latency carbon budget analysis reveals a large decline of the land carbon sink in 2023. Natl. Sci. Rev. 11, nwae367 (2024). https://doi.org/10.1093/nsr/nwae367

Gui, Y. et al. The decline in tropical land carbon sink drives high atmospheric CO₂ growth rate in 2023. Natl. Sci. Rev. nwae365 (2024). https://doi.org/10.1093/nsr/nwae365

Xia, L., Liu, R., Fan, W. et al. Emerging carbon dioxide hotspots in East Asia identified by a top-down inventory. Commun Earth Environ 6, 10 (2025). https://doi.org/10.1038/s43247-024-01991-7

Pani, S.K. et al. Long-term observation of columnar aerosol optical properties over the remote South China Sea. Sci. Total Environ. 905, 167113 (2023). https://doi.org/10.1016/j.scitotenv.2023.167113

Buchholz, R. R. et al. Air pollution trends measured from Terra: CO and AOD over industrial, fire-prone, and background regions. Remote Sensing Environ. 256, 112275 (2021). https://doi.org/10.1016/j.rse.2020.112275

Cui, D.Y. et al. Impact of atmospheric wet deposition on phytoplankton community structure in the South China Sea. Estuar. Coast. Shelf Sci. 173, 1–8 (2016). https://doi.org/10.1016/j.ecss.2016.02.011

Lin, N.-H. et al. An overview of regional experiments on biomass burning aerosols and related pollutants in Southeast Asia: from BASE-ASIA and the Dongsha Experiment to 7-SEAS. Atmos. Environ. 78, 1–19 (2013). https://doi.org/10.1016/j.atmosenv.2013.04.066

Reid, J. S. et al. Observing and understanding the Southeast Asian aerosol system by remote sensing: an initial review and analysis for the Seven Southeast Asian Studies (7SEAS) program. Atmos. Res. 122, 403–468 (2013). https://doi.org/10.1016/j.atmosres.2012.06.005

Lee, C.-T. et al. Aerosol chemical profile of near-source biomass burning smoke in Sonla, Vietnam during 7-SEAS campaigns in 2012 and 2013. Aerosol Air Qual. Res. 16, 2603–2617 (2016). https://doi.org/10.4209/aaqr.2015.07.0465

Tsay, S.-C. et al. Satellite-surface perspectives of air quality and aerosol-cloud effects on the environment: An overview of 7-SEAS/BASELInE. Aerosol Air Qual. Res. 16, 2581–2602 (2016). https://doi.org/10.4209/aaqr.2016.08.0350

Huang, H.-Y. et al. Influence of synoptic-dynamic meteorology on the long-range transport of Indochina biomass burning aerosols. J. Geophys. Res. Atmos. 125, e2019JD031260 (2020). https://doi.org/10.1029/2019JD031260

Ou-Yang, C.F. et al. Detection of stratospheric intrusion events and their role in ozone enhancement at a mountain background site in sub-tropical East Asia. Atmos. Environ. 268, 118779 (2022). https://doi.org/10.1016/j.atmosenv.2021.118779

Alexander, L. Extreme heat rooted in dry soils. Nature Geosci 4, 12–13 (2011). https://doi.org/10.1038/ngeo1045

Fischer, E. M., Seneviratne, S. I., Vidale, P. L., Lüthi, D. & Schär, C. M. Soil Moisture–Atmosphere Interactions during the 2003 European Summer Heat Wave. J. Clim. 20, 5081–5099 (2007). https://doi.org/10.1175/JCLI4288.1

Dong, Z., Yang, R., Cao, J., Wang, L. & Cheng, J. A strong high-temperature event in late-spring 2023 in Yunnan province, Southwest China: Characteristics and possible causes. Atmos. Res 295, 107017 (2023). https://doi.org/10.1016/j.atmosres.2023.107017

Ma, T. et al. Attribution analysis of the persistent and extreme drought in southwest China during 2022–2023. Environ. Res. Lett. 19, 114056 (2024).

Wai, K. M., Lin, N.-H., Wang, S.-H., and Dokiya, Y. Rainwater chemistry at a high altitude station, Mt. Lulin, Taiwan: comparison with a background station, Mt. Fuji, J. Geophy. Res. 113, D06305 (2008). doi:10.1029/2006JD008248.

Lin, C. Y. et al. A new transport mechanism of biomass burning from Indochina as identified by modeling studies. Atmos. Chem. Phys. 9, 7901–7911 (2009). https://doi.org/10.5194/acp-9-7901-2009

Chuang, M.T. et al. Carbonaceous aerosols in the air masses transported from Indochina to Taiwan: Long-term observation at Mt. Lulin. Atmos. Environ. 89, 507–516 (2014). https://doi.org/10.1016/j.atmosenv.2013.11.066

Lin, C.C. et al. Influences of the long-range transport of biomass-burning pollutants on surface air quality during 7-SEAS field campaigns. Aerosol Air Qual. Res. 17, 2595–2607 (2017). https://doi.org/10.4209/aaqr.2017.08.0273

Ou-Yang, C.F. et al. Characteristics of atmospheric carbon monoxide at a high-mountain background station in East Asia. Atmos. Environ. 89, 613–622 (2014). https://doi.org/10.1016/j.atmosenv.2014.02.060

Pani, S.K. et al. Relationship between long-range transported atmospheric black carbon and carbon monoxide at a high-altitude background station in East Asia. Atmos. Environ. 210, 86–99 (2019). https://doi.org/10.1016/j.atmosenv.2019.04.053

Ravindra Babu, S. et al. Transport pathways of carbon monoxide from Indonesian fire pollution to a subtropical high-altitude mountain site in the western North Pacific. Atmos. Chem. Phys. 23, 4727–4740 (2023). https://doi.org/10.5194/acp-23-4727-2023

Huang, H.-Y. et al. Impact of regional climate patterns on the biomass burning emissions and transport over Peninsular Southeast Asia, 2000–2019. Atmos. Res. 297, 107067 (2024). https://doi.org/10.1016/j.atmosres.2023.107067

Hu, Y., Yue, X. & Tian, C. Climatic drivers of the Canadian wildfire episode in 2023. Atmos. Oceanic Sci. Lett. 17, 100483 (2024). https://doi.org/10.1016/j.aosl.2024.100483

https://doi.org/10.5194/egusphere-2025-4223
Preprint. Discussion started: 4 September 2025

Sheu G.-R., N.-H. Lin, J.-L. Wang, C.-T. Lee. Temporal distribution and potential sources of atmospheric mercury measured at a high-elevation background station in Taiwan. Atmos. Environ. 44, 2393-2400 (2010).

Gill, A. E. Some simple solutions for heat-induced tropical circulation. Q. J. R. Meteorol. Soc. 106, 447–462 (1980). https://doi.org/10.1002/qj.49710644905

Zeng, Z. & Sun, J. Impacts of a tripolar sea surface temperature pattern over tropical–North Pacific on interannual variations of spring extreme consecutive dry days over southern China. J. Geophys. Res. Atmos. 127, e2021JD036281 (2022). https://doi.org/10.1029/2021JD036281

Jaffe, D. A. & Wigder, N. L. Ozone production from wildfires: a critical review. Atmos. Environ. 51, 1–10 (2012). https://doi.org/10.1016/j.atmosenv.2011.11.063

Ogino, S.-Y. et al. Cause of a lower-tropospheric high-ozone layer in spring over Hanoi. J. Geophys. Res. Atmos. 127, e2021JD035727 (2022). https://doi.org/10.1029/2021JD035727

Liu, H. et al. Sources of tropospheric ozone along the Asian Pacific Rim: An analysis of ozonesonde observations. J. Geophys. Res. 107, ACH31–ACH319 (2002). https://doi.org/10.1029/2001JD002005

Chan, C.Y. et al. Characteristics of biomass burning emission sources, transport, and chemical speciation in enhanced springtime tropospheric ozone profile over Hong Kong. J. Geophys. Res. 108, 1– (2003). https://doi.org/10.1029/2001jd001555

Ou-Yang, C.F. et al. Seasonal and diurnal variations of ozone at a high-altitude mountain baseline station in East Asia. Atmos. Environ. 46, 279–288 (2012). https://doi.org/10.1016/j.atmosenv.2011.09.060

Yadav, I.C. et al. Biomass burning in Indo-China peninsula and its impacts on regional air quality and global climate change—a review. Environ. Pollut. 227, 414–427 (2017). https://doi.org/10.1016/j.envpol.2017.04.085

Liao, Z. et al. Tropospheric ozone variability over Hong Kong based on recent 20-year (2000–2019) ozonesonde observation. J. Geophys. Res. Atmos. 126, e2020JD033054 (2021). https://doi.org/10.1029/2020jd033054

Zachariah, M. et al. Extreme humid heat in South and Southeast Asia in April 2023, largely driven by climate change, detrimental to vulnerable and disadvantaged communities. World Weather Attribution (2023). Available at: https://spiral.imperial.ac.uk/bitstream/10044/1/104092/18/south%20asia%20heat%20scientific%20report.pdf

Lyu, Y. et al. The characterization, mechanism, predictability, and impacts of the unprecedented 2023 Southeast Asia heatwave. npj Clim. Atmos. Sci. 7, 246 (2024). https://doi.org/10.1038/s41612-024-00797-w

Platnick, S., King, M. & Hubanks, P. MODIS Atmosphere L3 Monthly Product. https://doi.org/10.5067/MODIS/MOD08_M3.006 (2015).

Buchholz, R. R. et al. Air pollution trends measured from Terra: CO and AOD over industrial, fire-prone, and background regions. Remote Sensing Environ. 256, 112275 (2020). https://doi.org/10.1016/j.rse.2020.112275

Giglio, L., Csiszar, I. & Justice, C. O. Global distribution and seasonality of active fires as observed with the Terra and Aqua MODIS sensors. J. Geophys. Res. Biogeosci. 111, G02016 (2006). https://doi.org/10.1029/2005JG000142

Giglio, L., Schroeder, W. & Justice, C. O. The Collection 6 MODIS active fire detection algorithm and fire products. Remote Sens. Environ. 178, 31–41 (2016). https://doi.org/10.1016/j.rse.2016.02.054

Giglio, L., Boschetti, L., Roy, D. P., Humber, M. L. & Justice, C. O. The Collection 6 MODIS burned area mapping algorithm and product. Remote Sens. Environ. 217, 72–85 (2018). https://doi.org/10.1016/j.rse.2018.08.005

Worden, H. M. et al. Observations of near-surface carbon monoxide from space using MOPITT multispectral retrievals. J. Geophys. Res.: Atmos. 115, (2010). https://doi.org/10.1029/2010JD014242

Deeter, M. N. et al. Radiance-based retrieval bias mitigation for the MOPITT instrument: the version 8 product. Atmos. Meas. Tech. 12, 4561–4580 (2019). https://doi.org/10.5194/amt-12-4561-2019

McMillan, W. W. et al. Daily global maps of carbon monoxide from NASA's Atmospheric Infrared Sounder. Geophys. Res. Lett. 32 (2005). https://doi.org/10.1029/2004GL021821

Warner, J. X. et al. A comparison of satellite tropospheric carbon monoxide measurements from AIRS and MOPITT during INTEX-A. J. Geophys. Res. 112, D12S17 (2007). https://doi.org/10.1029/2006JD007925

Warner, J. et al. Tropospheric carbon monoxide variability from AIRS under clear and cloudy conditions. Atmos. Chem. Phys. 13, 12469–12479 (2013). https://doi.org/10.5194/acp-13-12469-2013

McMillan, W. W. et al. Validating the AIRS Version 5 CO retrieval with DACOM in situ measurements during INTEX-A and -B. IEEE Trans. Geosci. Remote Sens. 49, 2802–2813 (2011). https://doi.org/10.1109/TGRS.2011.2106505

AIRS Project. Aqua/AIRS L3 Monthly Standard Physical Retrieval (AIRS-only) 1 degree × 1 degree V7.0. Goddard Earth Sciences Data and Information Services Center (GES DISC), Greenbelt, MD, USA (2019). https://doi.org/10.5067/UBENJB9D3T2H

Ziemke, J. R. et al. Trends in global tropospheric ozone inferred from a composite record of TOMS/OMI/MLS/OMPS satellite measurements and the MERRA-2 GMI simulation. Atmos. Chem. Phys. 19, 3257–3269 (2019). https://doi.org/10.5194/acp-19-3257-2019

Ziemke, J. R. et al. Tropospheric ozone determined from Aura OMI and MLS: evaluation of measurements and comparison with the Global Modeling Initiative's Chemical Transport Model. J. Geophys. Res. 111, D19303 (2006). https://doi.org/10.1029/2006JD007089.

Cooper, O. R. et al. Increasing springtime ozone mixing ratios in the free troposphere over western North America. Nature 463, 344–348 (2010). https://doi.org/10.1038/nature08708

Gaudel, A. et al. Tropospheric Ozone Assessment Report: Present-day distribution and trends of tropospheric ozone relevant to climate and global atmospheric chemistry model evaluation. Elem. Sci. Anth. 6, 39 (2018). https://doi.org/10.1525/elementa.291

Lu. et al. An evaluation of the ability of the Ozone Monitoring Instrument (OMI) to observe boundary layer ozone pollution across China: application to 2005–2017 ozone trends. Atmos. Chem. Phys. 19, 6551–6560 (2019). https://doi.org/10.5194/acp-19-6551-2019

Gelaro, R. et al. The modern-era retrospective analysis for research and applications, Version 2 (MERRA-2). J. Clim. 30, 5419–5454 (2017). https://doi.org/10.1175/JCLI-D-16-0758.1